Proceedings of the International Conference on Oxide Materials for Electronic Engineering (OMEE 2021)

(Y, Gd)AlO_3 Perovskite Single Crystals Doped with Mn^{2+} Ions

V. Stasiv[a,*], M. Głowacki[a], J. Fink-Finowicki[a], Ya. Zhydachevskyy[a,b], S. Ubizskii[b], M. Berkowski[a] and A. Suchocki[a]

[a] *Institute of Physics, Polish Academy of Sciences, Aleja Lotników 32/46, PL-02668 Warsaw, Poland*
[b] *Lviv Polytechnic National University, Bandera Str. 12, 79013 Lviv, Ukraine*

Doi: 10.12693/APhysPolA.141.374 *e-mail: stasiv@ifpan.edu.pl

The work presents an experimental study of (Y, Gd)AlO_3:Mn^{2+} crystals grown by the Czochralski method under inert gas atmosphere and by the floating-zone method in the ambient air atmosphere. The Mn^{2+}/Mn^{4+} ratio, the energy depth of the main dosimetric and shallow traps are analyzed in comparison with the $YAlO_3$:Mn^{2+} and (Y, Lu)AlO_3:Mn^{2+} crystals studied before.

topics: thermoluminescence, optically stimulated luminescence, (Y, Gd)AlO_3:Mn, trap depth

1. Introduction

Mn^{2+}-doped $YAlO_3$ (YAP) crystals have proven to be good candidates for thermoluminescent (TL) or optically stimulated luminescent (OSL) dosimetry of ionizing radiation (see [1] and references therein). This material, having a high effective atomic number ($Z_{eff} \sim 31.4$), is of particular interest for the purposes of estimating the energy range of unknown photon radiation fields [2].

It is well known that the effect of shallow traps (the traps shallower than the ones used for dosimetry) in the case of TL readout can be easily eliminated by preheating the detectors to a certain temperature, which does not affect the main dosimetric TL peak. For the $YAlO_3$:Mn^{2+} crystals with the main TL peak at about 200°C, a short preheating to 120°C is appropriate [3]. However, in the case of OSL readout, the presence of shallow traps can considerably affect the OSL decay curves [4, 5]. The negative effect of shallow traps can be eliminated by decreasing the band gap of the host material by changing the chemical composition of the material [6, 7]. The decrease of the band gap of $YAlO_3$ perovskite can be achieved, e.g., by replacing Y with Gd [8]. Therefore, it was decided to grow the (Y, Gd)AlO_3:Mn^{2+} crystals and compare them with the $YAlO_3$:Mn^{2+} crystals studied before.

When getting manganese ions in $YAlO_3$ in the desired 2^+ valence state, a codoping with Si^{4+} or Hf^{4+} proved to be efficient charge compensation [9]. However, even in such codoped crystals some residual amount of Mn^{4+} ions is present. Getting the as large as possible Mn^{2+}/Mn^{4+} ratio in the dosimetric $YAlO_3$:Mn^{2+} crystals becomes very important as the Mn^{4+} ions are responsible for deep traps (deeper than dosimetric ones) and UV light response of the material (see [9] for details). It is known that the presence of deeper traps can complicate a reliable dose readout in both TL and OSL modes [10, 11]. Consequently, the possibility to control the segregation of the Mn^{2+} and Mn^{4+} ions in $YAlO_3$ is of key importance.

In this paper, we investigate (Y, Gd)AlO_3:Mn^{2+} crystals grown by the Czochralski method under inert gas atmosphere and by the floating-zone method in the ambient air atmosphere. The crystals have been characterized by photoluminescence (PL), radioluminescence (RL), and thermoluminescence (TL) techniques. Our focus is on the Mn^{2+}/Mn^{4+} ratio, main dosimetric traps, shallow traps, as well as on the comparison of the investigated crystals with $YAlO_3$:Mn^{2+} and (Y, Lu)AlO_3:Mn^{2+} crystals studied before [12, 13].

2. Experimental procedures

Studied (Y, Gd)AlO_3:Mn^{2+} crystals were grown by the floating-zone (FZ) method. For this purpose, the appropriate amounts of raw material powders of Y_2O_3 (5N), Gd_2O_3 (5N), Al_2O_3 (spec. pure), HfO_2 (2N8) and MnO (4N) were calcinated at 1000 °C, then mixed, compacted into pellets and sintered two times for 6 h at 1600°C in air with intermediate grinding. Subsequently, the pellets were milled, and the resulting powder was then pressed to form a feed rod with a diameter of 8 mm and a length of 90 mm. This rod was further sintered at 1550°C for 12 h

in air. An optical furnace (type URN-2-3Pm made by the Moscow Power Engineering Institute) with two ellipsoidal mirrors and a 4.5 kW xenon lamp as a heat source was used for crystallization. The feed rod and the growing crystal were rotated in opposite directions to make heating uniform and force convection in the melting zone. The growth rate was 1 mm/h. In some experiments, an additional afterheater was used for lowering the temperature gradients in the growing crystal. In such a way, a number of (Y–Gd)AlO_3:Mn,Hf crystals have been obtained. Two of them, namely

- the stoichiometric $Y_{0.8}Gd_{0.2}AlO_3$:Mn(0.05%),Hf(0.5%) (denoted as FZ#1)

  and
- the yttrium-rich $Y_{1.02}Al_{0.975}O_3$:Mn(0.05%),Hf(0.2%) (denoted as FZ#13), see Fig. 1

grown in air, were studied in detail in the present work. After it was revealed that HfO_2 (2N8) oxide is a source of unintentional Fe^{2+} impurity (see [14] for details), the crystal FZ#13 was prepared using high-purity HfO_2 (4N5). The crystals were cut into slices 1 mm thick using a diamond wheel saw.

(Y–Gd)AlO_3 crystals with the same nominal content of dopants were also grown by the Czochralski method. Crystals were grown from the same raw materials (including HfO_2 (2N8)) using a pure N_2 gas atmosphere as described in [9]. In particular, two crystals of the nominal compositions

- $(Y_{0.875}Gd_{0.125})_{1.02}Al_{0.98}O_3$:Mn(0.05%),Hf(0.2%) (denoted as CZ#39)

  and
- $(Y_{0.85}Gd_{0.15})_{1.02}Al_{0.98}O_3$:Mn(0.05%),Hf(0.2%) (denoted as CZ#40) see Fig. 1

were studied. Besides, the Mn^{2+}-doped crystals, such as

- $Y_{1.02}Al_{0.98}O_3$:Mn(0.05%),Si(0.2%) (denoted as CZ#15) [13],
- $Y_{1.02}Al_{0.98}O_3$:Mn(0.05%),Hf(0.2%) (denoted as CZ#31) [1, 8]

  and
- $(Y_{0.8}Lu_{0.2})_{1.02}Al_{0.98}O_3$:Mn(0.05%),Hf(0.2%) (denoted as CZ#34) [14] reported previously,

were also studied for comparison.

For X-ray irradiation, a Hamamatsu 130 kV Microfocus X-Ray Source L9181-02 was used. The samples were irradiated and stored in darkness to avoid optical bleaching of the samples.

PL measurements were performed with the use of a Horiba/Jobin-Yvon Fluorolog-3 spectrofluorometer with a 450 W continuous xenon lamp as an excitation source and a Hamamatsu R928P photomultiplier detector in photon counting mode. The same spectrometer was also used for RL measurements under X-ray excitation.

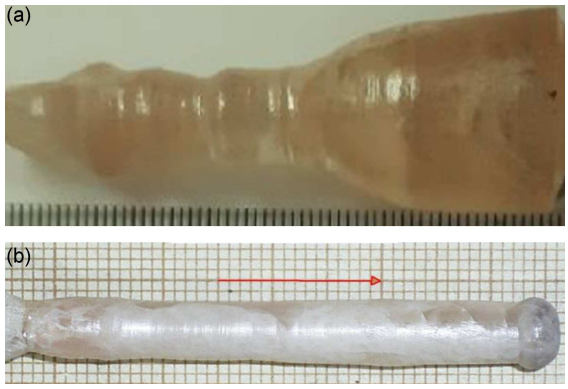

Fig. 1. Typical view of (Y, Gd)AlO_3:Mn,Hf crystals grown by the Czochralski (CZ#40) (a) and the floating-zone (FZ#13) (b) methods.

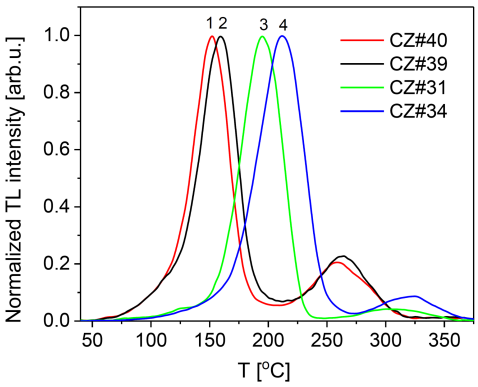

Fig. 2. Thermal glow curves of X-ray irradiated (Y–Gd)AP:Mn,Hf (CZ#40) (1), (Y–Gd)AP:Mn,Hf (CZ#39) (2), YAP:Mn,Hf (CZ#31) (3), and (Y–Lu)AP:Mn,Hf (CZ#34) (4) crystals recorded at 530 nm with a heating rate of 2 °C/s.

TL measurements above room temperature were done using a laboratory TL-reader with a Hamamatsu R928 photomultiplier. A blue-green bandpass filter (cutting off wavelengths > 600 nm) and a red longpass filter (cutting off < 650 nm) were used for TL measurements in green and red spectral ranges, respectively.

3. Experimental results and discussion

Thermal glow curves of some of the investigated crystals are presented in Fig. 2. As it is clearly seen, the partial replacement of Y by Gd shifts the main TL peak position towards low temperatures, whereas replacement by Lu, on the contrary, shifts its position towards higher temperatures, which is consistent with the results reported in [8, 13].

Trap depths estimated by the initial rise method for selected crystals are presented in Fig. 3. As it is clearly seen, the main dosimetric TL peak for the YAP:Mn,Hf (CZ#31) crystal possesses two activation energies of about 1.6 and 1.7 eV.

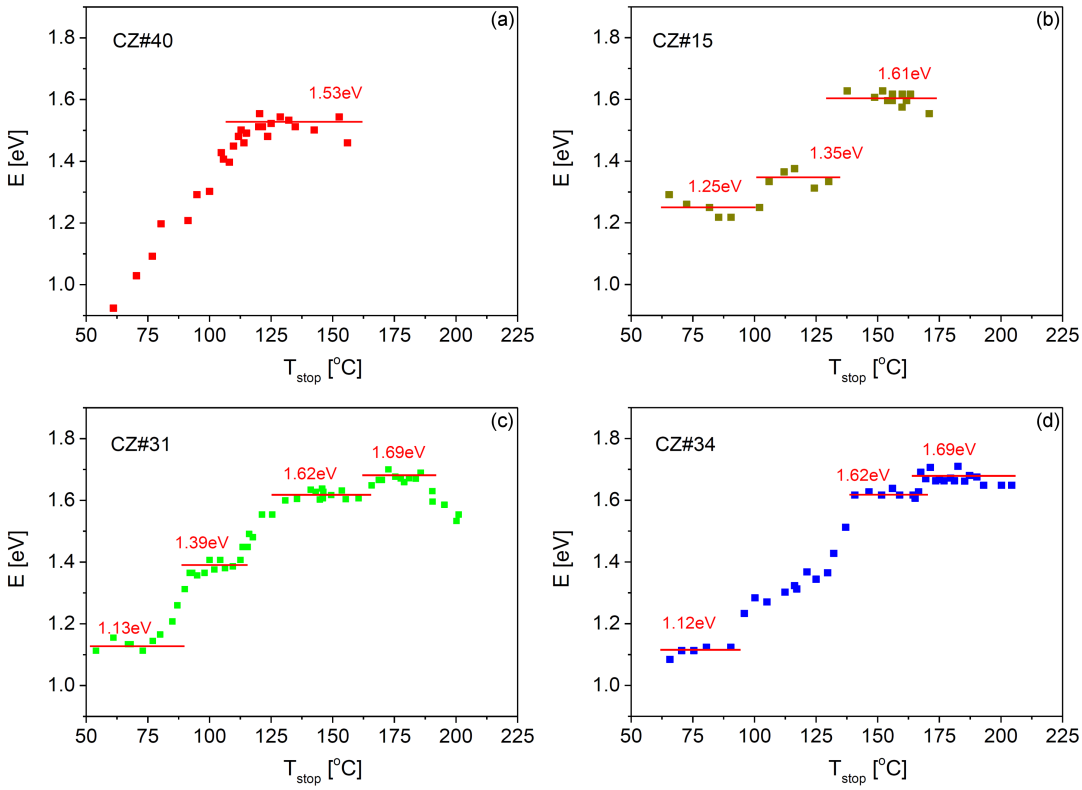

Fig. 3. Trap depths estimated by the initial rise method in the partial thermal cleaning procedure applied for the (Y–Gd)AP:Mn,Hf (CZ#40) (a), YAP:Mn,Si (CZ#15) (b), YAP:Mn,Hf (CZ#31) (c), and (Y–Lu)AP:Mn,Hf (CZ#34) (d) crystals.

The (Y–Lu)AP:Mn,Hf (CZ#34) crystal has the same activation energies, but the 1.7 eV component dominates, which apparently gives the shift in the TL peak position towards higher temperatures. For the (Y–Gd)AP:Mn,Hf (CZ#40) crystal, the activation energy of the main TL peak is about 1.5 eV. It is worth noting that the YAP:Mn,Si (CZ#15) crystal, which has an evidently narrower main TL peak compared to CZ#31 (see Fig. 4), has a single activation energy of about 1.6 eV. Each of the studied crystals has shallow traps responsible for the TL glow above 50 °C with activation energies of ≥ 1.0 eV. As it is seen in Fig. 3, the replacement of Y by Lu or Gd does not have any significant effect on the presence and depths of shallow traps.

The thermal glow registration separately in the green and red spectral ranges (see Fig. 4) allows separating the light output caused by Mn^{2+} and Mn^{4+} ions (see [14] for details). It was revealed that all the investigated crystals grown by the floating-zone method had a higher relative intensity of the parasitic Mn^{4+}-related red emission than the crystals obtained by the Czochralski method at the same nominal concentration of MnO and HfO_2 oxides in raw materials. It could probably be caused by the air atmosphere applied in FZ growth. According to the criterion of Mn^{2+}/Mn^{4+} emission ratio, the best result among all FZ crystals was achieved for the FZ#13 crystal (see Fig. 4c).

The afterglow decay curves observed just after switching off the X-ray excitation are shown in Fig. 5. The afterglow shows a rapid decay (with ms decay time commensurable with the Mn^{2+} photoluminescence decay), after which a long-lasting afterglow caused apparently by the shallow traps is observed. It should be noted that the replacement of Y by Lu or Gd does not have a significant effect on the shape of the afterglow. In particular, the initial intensity of the long afterglow is about 1/10 with respect to the intensity of the steady-state radioluminescence for the CZ#31, CZ#34, and CZ#39 crystals, which is consistent with the results presented in Fig. 3. The lowest relative intensity of the long afterglow (about 1/100 with respect to the steady-state RL level) was found for the Si-codoped CZ#15 crystal, which possesses a noticeably larger depth of shallow traps of about 1.25 eV.

Both photoluminescende and radioluminescence measurements (see Fig. 6 and Fig. 7) reveal that the intensity ratio of the green and red emission changes significantly along with the crystal. At this point, it should be noted that the green emission of Mn^{2+} ions under resonant optical excitation is relatively weak because all excitation transitions from the ground sextet level to higher quartet or doublet levels of Mn^{2+} are spin-forbidden. Nevertheless, green photoluminescence of Mn^{2+}

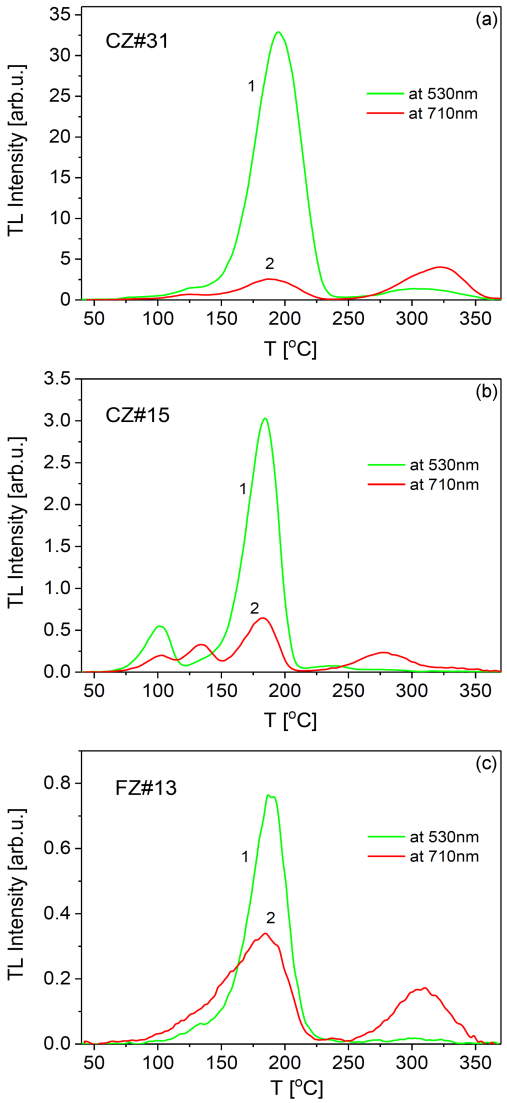

Fig. 4. Thermal glow curves of X-ray irradiated YAP:Mn,Hf (CZ#31) (a), YAP:Mn,Si (CZ#15) (b), and YAP:Mn,Hf (FZ#13) (c) crystals recorded at 530 nm (1) and 710 nm (2) with a heating rate of 2 °C/s.

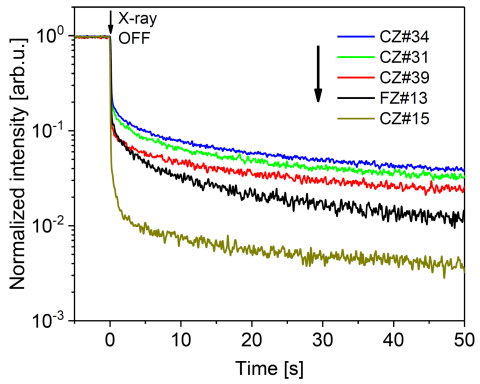

Fig. 5. Afterglow decay kinetics measured for selected crystals at 530 nm at room temperature after X-ray irradiation.

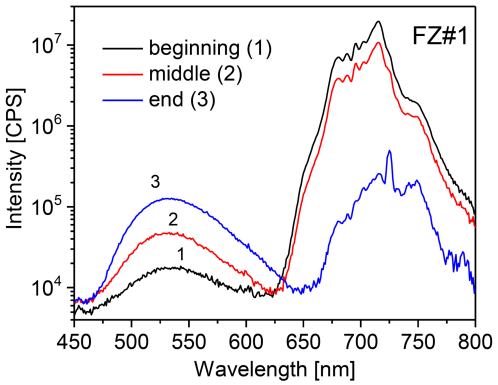

Fig. 6. Photoluminescence spectra of different parts of the (Y–Gd)AP:Mn,Hf (FZ#1) crystal measured under 414 nm excitation at room temperature.

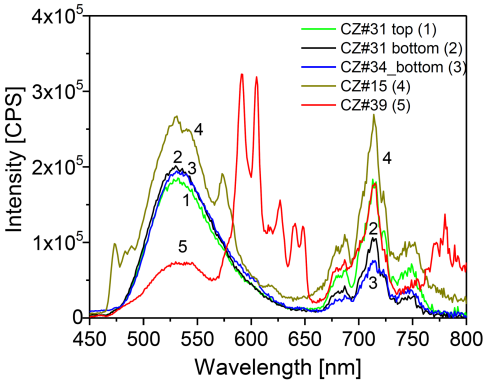

Fig. 7. Radioluminescence spectra of selected crystals measured under X-ray excitation at room temperature.

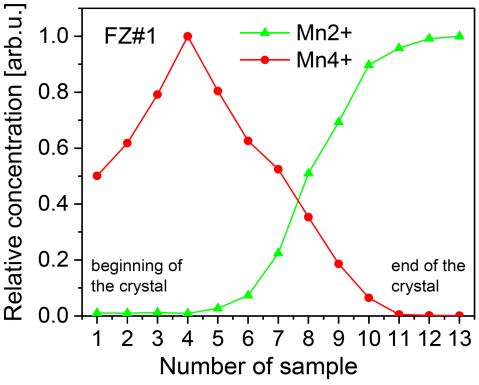

Fig. 8. Relative changes of the Mn^{2+} and Mn^{4+} ions concentration along a crystal derived from the photoluminescence measurements for the (Y–Gd)AP:Mn,Hf (FZ#1) crystal.

in YAP can still be measured under 414 nm excitation ($^6A_1 \rightarrow {}^4E + {}^4A_1$ transitions of Mn^{2+}) [1, 14]. In contrast, red photoluminescence of Mn^{4+} ions caused by the $^2E \rightarrow {}^4A_2$ transition is very efficient. Mn^{2+} ions can be excited more efficiently by ionizing irradiation (see [14] for details).

Analysis of integral PL or RL intensity separately for Mn^{2+} and Mn^{4+} ions allows following their relative change along the crystal, as shown in Fig. 8. Here, the sample's number corresponds to the sequence number of the sample taken along the crystal from the beginning to the end. As one can see in Fig. 8, the maximal Mn^{2+}/Mn^{4+} ratio due to particular segregation of the dopants occurs in the end part of the crystal. The same effect of Mn^{2+} and Mn^{4+} ions segregation, however much less pronounced, was also observed for the crystals grown by the Czochralski method (see Fig. 7, for instance).

4. Conclusions

Various kinds of (Lu, Y, Gd)AlO_3:Mn^{2+},Si(Hf) crystals grown by the Czochralski (CZ) and the floating-zone (FZ) techniques have been studied. The Mn^{2+}/Mn^{4+} concentration ratio was found to increase along a crystal (both from CZ and FZ technique) from the beginning to the end due to the segregation of the dopants.

The band-gap engineering (in our case, a partial replacement of Y by Lu or Gd) allows to significantly change the temperature of the main TL peak position in the (Lu, Y, Gd)AP:Mn^{2+} crystals via changing the energy depths of the main traps.

At the same time, it was revealed that the partial replacement of Y by Lu or Gd does not significantly influence the presence of shallow traps responsible for the afterglow of the crystals at room temperature. A much greater influence on the afterglow was found for various codopants used (Si^{4+} or Hf^{4+}). In particular, the Si-codoped crystals revealed a much lower relative intensity of the long afterglow (about 1/100 with respect to the steady-state radioluminescence), which is consistent with the larger depth of shallow traps in the crystals.

Acknowledgments

The work was supported by the Polish National Science Centre (project no. 2018/31/B/ST8/00774), by the Ministry of Education and Science of Ukraine (project DB/Kinetyka no. 0119U002249), and by the NATO SPS Project G5647.

References

[1] Ya. Zhydachevskii, A. Luchechko, D. Maraba, N. Martynyuk, M. Glowacki, E. Bulur, S. Ubizskii, M. Berkowski, A. Suchocki, *Radiat. Meas.* **94**, 18 (2016).

[2] V. Chumak, A. Morgun, Ya. Zhydachevskii, S. Ubizskii, V. Voloskiy, O. Bakhanova, *Radiat. Meas.* **106**, 638 (2017).

[3] Ya. Zhydachevskii, I. Kaminska, M. Berkowski, A. Twardak, P. Bilski, S. Ubizskii, A. Suchocki, in: *Proc. Int. Conf. on Oxide Materials for Electronic Engineering — Fabrication, Properties and Applications (OMEE-2014)*, IEEE, Lviv 2014, p. 261.

[4] C. Ankjaergaard, M. Jain, *J. Phys. D: Appl. Phys.* **43**, 255502 (2010).

[5] G. Denis, M.S. Akselrod, E.G. Yukihara, *J. Appl. Phys.* **109**, 104906 (2011).

[6] M. Fasoli, A. Vedda, M. Nikl, C. Jiang, B.P. Uberuaga, D.A. Andersson, K.J. McClellan, C.R. Stanek, *Phys. Rev. B* **84**, 081102(R) (2011).

[7] I.I. Vrubel, R.G. Polozkov, I.A. Shelykh, V.M. Khanin, P.A. Rodnyi, C.R. Ronda, *Cryst. Growth Design* **17**, 1863 (2017).

[8] Ya. Zhydachevskyy, Yu. Hizhnyi, S.G. Nedilko et al., *J. Phys. Chem. C* **125**, 26698 (2021).

[9] Ya. Zhydachevskii, A. Suchocki, M. Berkowski, D. Sugak, A. Luchechko, S. Warchol, *J. Cryst. Growth* **310**, 3219 (2008).

[10] E.G. Yukihara, V.H. Whitley, J.C. Polf, D.M. Klein, S.W.S. McKeever, A.E. Akselrod, M.S. Akselrod, *Radiat. Meas* **37**, 627 (2003).

[11] D. Van der Heggen, D. Vandenberghe, N.K. Moayed, J. De Grave, P.F. Smet, J.J. Joos, *J. Lumin.* **226**, 117496 (2020).

[12] Ya. Zhydachevskii, A. Suchocki, M. Berkowski, S. Warchol, *Acta Phys. Pol. A* **117**, 177 (2010).

[13] Ya. Zhydachevskii, M. Glowacki, N. Martynyuk, S. Ubizskii, M. Berkowski, A. Suchocki, *Acta Phys. Pol. A* **133**, 973 (2018).

[14] H. Przybylińska, Ya. Zhydachevskyy, A. Grochot, A. Wołoś, V. Stasiv, M. Glowacki, A. Kamińska, S. Ubizskii, M. Berkowski, A. Suchocki, *J. Phys. Chem. C* **126**, 743 (2022).